Synthesis and Electrochemical Studies of Diiron Complexes of 1,8-Naphthyridine-Based Dinucleating Ligands to Model Features of the Active Sites of Non-Heme Diiron Enzymes

Chuan He and Stephen J. Lippard*

Department of Chemistry, Massachusetts Institute of Technology, Cambridge, Massachusetts 02139

Received August 25, 2000

A bis(μ-carboxylato)(μ-1,8-naphthyridine)diiron(II) complex, $[Fe_2(BPMAN)(\mu\text{-}O_2CPhCy)_2](OTf)_2$ (**1**), was prepared by using the 1,8-naphthyridine-based dinucleating ligand BPMAN, where BPMAN = 2,7-bis[bis(2-pyridylmethyl)-aminomethyl]-1,8-naphthyridine. The cyclic voltammogram (CV) of this complex in CH_2Cl_2 exhibited two reversible one-electron redox waves at +296 mV (ΔE_p = 80 mV) and +781 mV (ΔE_p = 74 mV) vs Cp_2Fe^+/Cp_2Fe, corresponding to the $Fe^{III}Fe^{II}/Fe^{II}Fe^{II}$ and $Fe^{III}Fe^{III}/Fe^{III}Fe^{II}$ couples, respectively. This result is unprecedented for diiron complexes having no single atom bridge. Dinuclear complexes $[Fe_2(BPMAN)(\mu\text{-}OH)(\mu\text{-}O_2CPhCy)](OTf)_2$ (**2**) and $[Mn_2(BPMAN)(\mu\text{-}O_2CPhCy)_2](OTf)_2$ (**3**) were also synthesized and structurally characterized. The cyclic voltammogram of **2** in CH_2Cl_2 exhibited one reversible redox wave at −22 mV only when the potential was kept below +400 mV. The CV of **3** showed irreversible oxidation at potentials above +900 mV. Diiron(II) complexes $[Fe_2(BEAN)(\mu\text{-}O_2CPhCy)_3](OTf)$ (**4**) and $[Fe_2(BBBAN)(\mu\text{-}OAc)_2(OTf)](OTf)$ (**6**) were also prepared and characterized, where BEAN = 2,7-bis(*N*,*N*-diethylaminomethyl)-1,8-naphthyridine and BBBAN = 2,7-bis-{2-[2-(1-methyl)benzimidazolylethyl]-*N*-benzylaminomethyl}-1,8-naphthyridine. The cyclic voltammograms of these complexes were recorded. The Mössbauer properties of the diiron compounds were studied.

Introduction

The enzymes methane monooxygenase (MMO), ribonucleotide reductase (RNR), and Δ-9 desaturase (Δ9D) belong to a class of non-heme diiron-containing proteins that have been the subjects of extensive investigation in recent years.[1−4] Carboxylate-bridged diiron clusters at the active sites of these enzymes activate O_2 for different biological functions. The reduced forms of the proteins have been characterized by macromolecular X-ray crystallography.[5−7] They all contain diiron(II) units with carboxylate-only bridges at the active sites (Figure 1) that react with O_2 to give intermediates responsible for their respective functions. In at least one case, a diiron(II) center bridged only by carboxylate groups in ribonucleotide reductase was suggested to function as an electron supplier during enzyme turnover.[8]

Many carboxylate-bridged diiron(II) complexes have been prepared as models for the active sites of the reduced enzymes. Some of these complexes also react with O_2 to give intermediates that mimic features observed in the enzymatic systems.[9−15] These reactions all involve oxidation of the diiron centers. Knowledge of the redox potentials of diiron(II) complexes may help explain the O_2 reactivity in some cases. If outer sphere electron transfer from diiron(II) to O_2 were to occur as the first step, the oxidation potential of the diiron(II) core would determine the O_2 reactivity. It therefore would be valuable to understand how the redox properties of the synthetic model complexes varied with their compositions and structures. The study of the electrochemical behavior of diiron complexes is limited, however, due to decomposition pathways that occur under redox conditions.[16]

To address this problem, we have developed a series of new dinucleating ligands based on 1,8-naphthyridine. The 1,8-naphthyridine unit coordinates to and bridges two metal ions, as we have demonstrated previously.[17] Dimetallic compounds prepared from these "masked carboxylate" ligands exhibit a wide range of metal−metal separations and flexible geometry. Different oxidation states of the metal ions can be accommodated while still maintaining a stable dinuclear core.

In the present report we describe the synthesis and characterization of several diiron(II) compounds that contain the dinucleating ligands BPMAN, BEAN, and BBBAN,[18] where BPMAN = 2,7-bis[bis(2-pyridylmethyl)aminomethyl]-1,8-naphthyridine, BEAN = 2,7-bis(*N*,*N*-diethylaminomethyl)-1,8-naphthyridine, and BBBAN = 2,7-bis{2-[2-(1-methyl)benzimida-

(1) Solomon, E. I.; Brunold, T. C.; Davis, M. I.; Kemsley, J. N.; Lee, S.-K.; Lehnert, N.; Neese, F.; Skulan, A. J.; Yang, Y.-S.; Zhou, J. *Chem. Rev.* **2000**, *100*, 235−349.
(2) Valentine, A. M.; Lippard, S. J. *J. Chem. Soc., Dalton Trans.* **1997**, 3925−3931.
(3) Que, L., Jr. *J. Chem. Soc., Dalton Trans.* **1997**, 3933−3940.
(4) Wallar, B. J.; Lipscomb, J. D. *Chem. Rev.* **1996**, *96*, 2625−2657.
(5) Rosenzweig, A. C.; Nordland, P.; Takahara, P. M.; Frederick, C. A.; Lippard, S. J. *Chem. Biol.* **1995**, *2*, 409−418.
(6) Logan, D. T.; Su, X.-D.; Åberg, A.; Regnström, K.; Hajdu, J.; Eklund, H.; Nordlund, P. *Structure* **1996**, *4*, 1053−1064.
(7) Lindqvist, Y.; Huang, W.; Schneider, G.; Shanklin, J. *EMBO J.* **1996**, *15*, 4081−4092.
(8) Miller, M. A.; Gobena, F. T.; Kauffman, K.; Münck, E.; Que, L., Jr.; Stankovich, M. T. *J. Am. Chem. Soc.* **1999**, *121*, 1096−1097.
(9) Ménage, S.; Zang, Y.; Hendrich, M. P.; Que, L., Jr. *J. Am. Chem. Soc.* **1992**, *114*, 7786−7792.
(10) Kim, K.; Lippard, S. J. *J. Am. Chem. Soc.* **1996**, *118*, 4914−4915.
(11) Ookubo, T.; Sugimoto, H.; Nagayama, T.; Masuda, H.; Sato, T.; Tanaka, K.; Maeda, Y.; Okawa, H.; Hayashi, Y.; Uehara, A.; Suzuki, M. *J. Am. Chem. Soc.* **1996**, *118*, 701−702.
(12) Dong, Y.; Yan, S.; Young, V. G., Jr.; Que, L., Jr. *Angew. Chem., Int. Ed. Engl.* **1996**, *35*, 618−620.
(13) LeCloux, D. D.; Barrios, A. M.; Mizoguchi, T. J.; Lippard, S. J. *J. Am. Chem. Soc.* **1998**, *120*, 9001−9014.
(14) Lee, D.; Du Bois, J.; Petasis, D.; Hendrich, M. P.; Krebs, C.; Huynh, B. H.; Lippard, S. J. *J. Am. Chem. Soc.* **1999**, *121*, 9893−9894.
(15) Hagadorn, J. R.; Que, L., Jr.; Tolman, W. B. *J. Am. Chem. Soc.* **1998**, *120*, 13531−13532.
(16) Armstrong, W. H.; Spool, A.; Papaefthymiou, G. C.; Frankel, R. B.; Lippard, S. J. *J. Am. Chem. Soc.* **1984**, *106*, 3653−3667.
(17) He, C.; Lippard, S. J. *J. Am. Chem. Soc.* **2000**, *122*, 184−185.
(18) He, C.; Lippard, S. J. *Tetrahedron* **2000**, *56*, 8245−8252.

10.1021/ic000975k CCC: $20.00 © 2001 American Chemical Society
Published on Web 01/13/2001

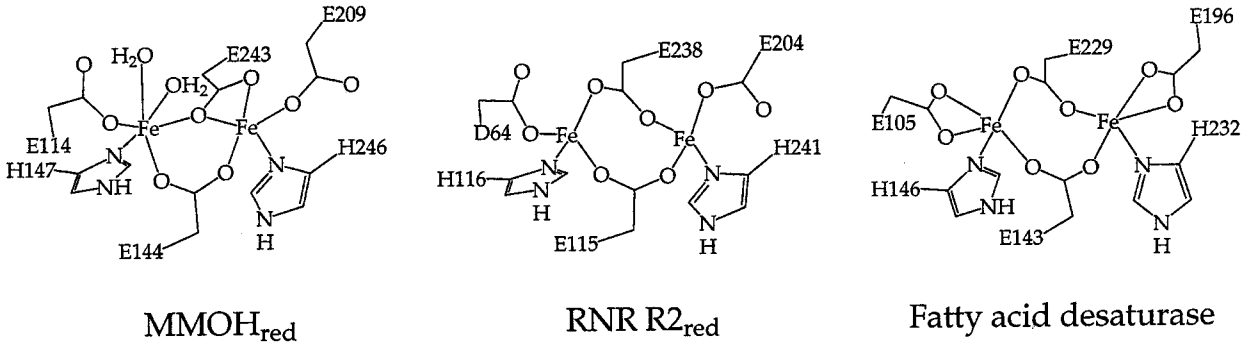

Figure 1. Schematic representation of the active site structures of reduced MMOH, RNR and Δ-9 desaturase.

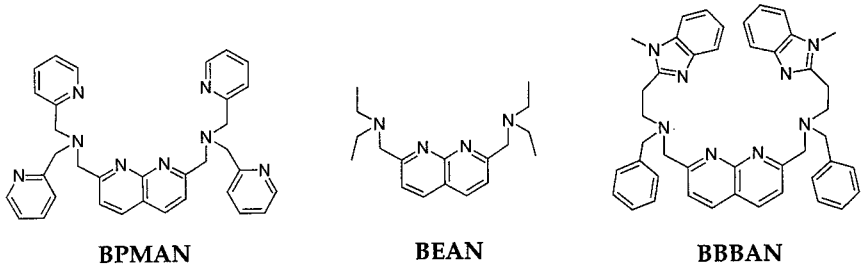

Figure 2. Schematic representation of ligands BPMAN, BEAN, and BBBAN.

zolylethyl]-*N*-benzylaminomethyl}-1,8-naphthyridine (Figure 2). A diiron complex containing additional carboxylate bridges, $[Fe_2(BPMAN)(\mu\text{-}O_2CPhCy)_2](OTf)_2$ (**1**), prepared with the use of BPMAN exhibited two reversible redox waves in a cyclic voltammetric experiment. The complexes $[Fe_2(BPMAN)(\mu\text{-}OH)(\mu\text{-}O_2CPhCy)](OTf)_2$ (**2**), $[Mn_2(BPMAN)(\mu\text{-}O_2CPhCy)_2](OTf)_2$ (**3**), $[Fe_2(BEAN)(\mu\text{-}O_2CPhCy)_3](OTf)$ (**4**), $[Fe_2(BEAN)(\mu\text{-}O_2CCPh_3)_3](OTf)$ (**5**), and $[Fe_2(BBBAN)(\mu\text{-}OAc)_2(OTf)](OTf)$ (**6**) were also synthesized and their cyclic voltammograms recorded. The Mössbauer properties of all the diiron compounds were studied as well.

Experimental Section

General Procedures and Methods. All reagents were obtained from commercial suppliers and used without further purification unless otherwise noted. THF was distilled from sodium benzophenone ketyl under nitrogen. Pentane and diethyl ether were purified by passage through activated alumina columns under nitrogen. Dichloromethane, acetonitrile, and propionitrile were distilled from CaH_2 under nitrogen. Fourier transform infrared spectra were recorded on a Bio-Rad FTS135 instrument and UV−vis spectra on a Varian 1-E spectrophotometer. Mössbauer spectra were recorded on an MS1 spectrometer (WEB Research Co.) with a ^{57}Co source in a Rh matrix maintained at room temperature in the MIT Department of Chemistry Instrumentation Facility. Ligands BPMAN, BEAN, and BBBAN were synthesized according to procedures reported elsewhere.[18] $Fe(OTf)_2{\cdot}2CH_3CN_3$, $Mn(OTf)_2{\cdot}2CH_3CN_3$, and 1-phenylcyclohexanecarboxylic acid were prepared by following known procedures.[19,20] All air-sensitive manipulations were carried out either in a nitrogen-filled Vacuum Atmospheres drybox or by standard Schlenk line techniques.

$[Fe_2(BPMAN)(\mu\text{-}O_2CPhCy)_2](OTf)_2$ (1). To a solution of $Fe(OTf)_2{\cdot}2CH_3CN_3$ (60 mg, 0.145 mmol) in acetonitrile (3 mL) was added sodium 1-phenylcyclohexanecarboxylate (33 mg, 0.145 mmol) and BPMAN (40 mg, 0.072 mmol). The mixture was allowed to stir for 1 h and the solvent was removed under vacuum. The residue was dissolved in CH_2Cl_2 and filtered. Crystallization from Et_2O/CH_2Cl_2 yielded blue blocks suitable for X-ray crystallography (62 mg, 63%). FTIR (KBr, cm^{-1}): 3070 (w), 2935 (s), 2859 (m), 1605 (s), 1593 (s), 1445 (m), 1396 (s), 1350 (w), 1276 (s), 1223 (m), 1152 (s), 1100 (w), 1031 (s), 905 (w), 793 (w), 766 (m), 736 (m), 702 (w), 637 (s). UV−vis (CH_2Cl_2, λ_{max}, nm (ϵ, M^{-1} cm^{-1})) 560 (660). Anal. Calcd for **1**, $C_{62}H_{62}N_8O_{10}S_2F_6Fe_2$: C, 54.48; H, 4.56; N, 8.18. Found: C, 54.36; H, 4.42; N, 8.23.

$[Fe_2(BPMAN)(\mu\text{-}OH)(\mu\text{-}O_2CPhCy)](OTf)_2$ (2). To a solution of $Fe(OTf)_2{\cdot}2CH_3CN_3$ (150 mg, 0.361 mmol) in acetonitrile (5 mL) was added sodium 1-phenylcyclohexanecarboxylate (41 mg, 0.181 mmol), BPMAN (100 mg, 0.181 mmol), Bu_3N (43 μL, 0.181 mmol), and water (5 μL). The mixture was allowed to stir for 1 h and the solvent was removed under vacuum. The residue was dissolved in CH_2Cl_2 and filtered. Crystallization from Et_2O/CH_2Cl_2 yielded green blocks suitable for X-ray crystallography (129 mg, 60%). FTIR (KBr, cm^{-1}): 3072 (m), 2932 (s), 2857 (m), 1604 (s), 1568 (s), 1513 (w), 1480 (m), 1445 (s), 1392 (s), 1349 (w), 1275 (s), 1224 (s), 1154 (s), 1100 (m), 1053 (w), 1031 (s), 978 (w), 960 (w), 906 (w), 888 (w), 867 (w), 848 (w), 793 (w), 764 (s), 737 (w), 702 (w), 637 (s). UV−vis (CH_2Cl_2, λ_{max}, nm (ϵ, M^{-1} cm^{-1})) 600 (569). Anal. Calcd for **2**, $C_{49}H_{48}N_8O_9S_2F_6Fe_2$: C, 49.76; H, 4.09; N, 9.47. Found: C, 49.66; H, 4.00; N, 9.59.

$[Mn_2(BPMAN)(\mu\text{-}O_2CPhCy)_2](OTf)_2$ (3). The procedure used to prepare **1** was followed except that $Mn(OTf)_2{\cdot}2CH_3CN_3$ was substituted as the metal salt. Compound **3** was obtained as yellow blocks from Et_2O/CH_2Cl_2 in 57% yield. Single crystals suitable for X-ray crystallography were grown at −30 °C from saturated EtO_2/CH_2Cl_2. FTIR (KBr, cm^{-1}): 3067 (w), 3033 (w), 2935 (s), 2859 (m), 1604 (s), 1590 (s), 1446 (m), 1401 (s), 1350 (w), 1277 (s), 1224 (m), 1152 (s),1099 (w), 1031 (s), 1015 (w), 905 (w), 793 (w), 766 (m), 736 (m), 702 (w), 637 (s). Anal. Calcd for **3**, $C_{62}H_{62}N_8O_{10}S_2F_6Mn_2$: C, 54.47; H, 4.57; N, 8.20. Found: C, 54.37; H, 4.36; N, 8.13.

$[Fe_2(BEAN)(\mu\text{-}O_2CPhCy)_3](OTf)$ (4). A portion of sodium 1-phenylcyclohexanecarboxylate (90.3 mg, 0.399 mmol) in THF (0.5 mL) was added to a solution of $Fe(OTf)_2{\cdot}2CH_3CN_3$ (109.7 mg, 0.266 mmol) in THF (1 mL). After 15 min of stirring, a portion of BEAN (40 mg, 0.133 mmol) in THF (1 mL) was added. The yellow solution was allowed to stir for 1 h and the solvent was removed under vacuum. The residue was dissolved in CH_2Cl_2 and filtered. Crystallization from pentane/Et_2O/CH_2Cl_2 yielded light yellow blocks suitable for X-ray crystallography (86 mg, 55%). FTIR (KBr, cm^{-1}): 3065 (m), 3040 (w), 3022 (w), 2978 (m), 2934 (s), 2862 (s), 1609 (s), 1579 (s), 1449 (s), 1396 (s), 1346 (m), 1277 (s), 1224 (m), 1149 (s), 1031 (s), 914 (m), 874 (m), 844 (m), 769 (m), 732 (s), 697 (m), 637 (s). Anal. Calcd for **4**, $C_{58}H_{73}N_4O_9SF_3Fe_2$: C, 59.49; H, 6.28; N, 4.78. Found: C, 59.37; H, 6.48; N, 4.79.

(19) Bryan, P. S.; Dabrowiak, J. C. *Inorg. Chem.* **1975**, *14*, 296−299.
(20) Calderon, S. N.; Newman, A. H.; Tortella, F. C. *J. Med. Chem.* **1991**, *34*, 3159−3164.

[Fe_2(BEAN)(μ-O_2CCPh_3)$_3$](OTf) (5). The same procedure to prepare **4** was followed, except that sodium triphenylacetate was used as the carboxylate group. Crystallization from pentane/Et_2O/benzene yielded **5** as light yellow blocks (32 mg, 22%). FTIR (KBr, cm^{-1}): 3060 (m), 3035 (w), 3022 (w), 2979 (m), 2944 (w), 2876 (w), 1610 (s), 1595 (s), 1571 (w), 1561 (m), 1542 (w), 1508 (w), 1492 (m), 1383 (s), 1277 (s), 1262 (s), 1223 (m), 1150 (s), 1031 (s), 870 (w), 768 (m), 637 (s). Anal. Calcd for **5**, $C_{79}H_{73}N_4O_9SF_3Fe_2$: C, 66.67; H, 5.17; N, 3.94. Found: C, 66.27; H, 5.18; N, 3.74.

[Fe_2(BBBAN)(μ-OAc)$_2$(OTf)](OTf) (6). A portion of BBBAN (30.3 mg, 0.044 mmol) in acetonitrile (2 mL) was added to a solution of $Fe(OTf)_2 \cdot 2CH_3CN_3$ (19 mg, 0.046 mmol) in acetonitrile (3 mL), followed by $Fe(OAc)_2$ (7.7 mg, 0.044 mmol). This solution was allowed to stir for 6 h and all the insoluble $Fe(OAc)_2$ powder dissolved. The color of the solution turned purple-pink. To this solution was added Et_2O until it became cloudy. The precipitates were filtered off. Layering Et_2O on top of the solution at −30 °C gave purple-pink plates suitable for X-ray crystallographic studies (22 mg, 41%). FTIR (KBr, cm^{-1}): 3065 (w), 3031 (w), 2959 (m), 2928 (m), 2876 (w), 1617 (m), 1612 (s), 1578 (m), 1571 (m), 1561 (m), 1523 (m), 1490 (m), 1458 (s), 1413 (m), 1332 (w), 1278 (s), 1224 (m), 1152 (s), 1031 (s), 892 (w), 857 (m), 796 (m), 753 (s), 707 (m), 638 (s). Anal. Calcd for **6**, $C_{50}H_{50}N_8O_{10}S_2F_6Fe_2$: C, 49.52; H, 4.16; N, 9.24. Found: C, 49.30; H, 4.35; N, 9.26.

X-ray Crystallography Studies. X-ray crystallographic studies were carried out on a Bruker (formerly Siemens) CCD diffractometer with graphite-monochromatized Mo Kα radiation ($\lambda = 0.71073$ Å) controlled by a Pentium-based PC running the SMART software package.[21] Single crystals were mounted at room temperature on the ends of quartz fibers in Paratone N oil, and data were collected at 193 K in a stream of cold N_2 maintained by a Bruker LT-2A nitrogen cryostat. Data collection and reduction protocols are described in detail elsewhere.[22] The structures were solved by direct methods and refined on F^2 by using the SHELXTL software package.[23] Empirical absorption corrections were applied with the SADABS program,[24] and the structures were checked for higher symmetry by PLATON.[25] All non-hydrogen atoms were refined anisotropically. Hydrogen atoms were assigned idealized locations and given isotropic thermal parameters 1.2 times the thermal parameter of the carbon atoms to which they were attached. In the structure of **2**, one triflate anion is disordered and was refined accordingly. In the structure of **6,** two half-occupied triflate anions were found in the lattice. A solvent acetonitrile molecule is half-occupied. Another acetonitrile molecule is disordered and was refined as C56 at 0.5 occupancy, C57(A) and N11(A) at 0.25 occupancy, and C57(B) and C11(B) at 0.25 occupancy.

Electrochemistry. Cyclic voltammetric measurements were performed in a Vacuum Atmospheres drybox under N_2 with an EG&G Model 263 potentiostat. A three-electrode configuration consisting of a 1.75 mm^2 platinum working electrode, a $Ag/AgNO_3$ (0.1 M in CH_3CN) reference electrode, and a coiled platinum wire auxiliary electrode was used. The supporting electrolyte was 0.5 M (Bu_4N)(PF_6). Sample concentrations of 2 mM were typically employed. All cyclic voltammograms were externally referenced to Cp_2Fe.

Mössbauer Spectroscopy. Powdered solid samples (~0.03 mol) were suspended in Apiezon N grease and packed into nylon sample holders in the drybox. The samples were removed from the drybox and rapidly precooled to 77 K. All data were collected at 4.2 K. Isomer shift (δ) values are reported with respect to iron foil that was used for velocity calibration at room temperature. The spectra were fit to Lorentzian lines by using the WMOSS plot and fit program.[26]

Results and Discussion

Preparation and Structural Characterization of [Fe_2(BPMAN)(μ-O_2CPhCy)$_2$](OTf)$_2$ (1), [Fe_2(BPMAN)(μ-OH)(μ-O_2CPhCy)](OTf)$_2$ (2) and [Mn_2(BPMAN)(μ-O_2CPhCy)$_2$](OTf)$_2$ (3). Compound **1** was prepared by reacting $Fe(OTf)_2 \cdot 2CH_3CN_3$, NaO_2CPhCy, and BPMAN in a 2:2:1 ratio in acetonitrile and crystallized as blue blocks from CH_2Cl_2/Et_2O at room temperature. The structure of **1** is shown in Figure 3, and selected bond lengths and angles are listed in Table 2. The two iron(II) atoms are bridged by two carboxylate groups and the 1,8-naphthyridine unit of BPMAN. Both iron atoms are six-coordinate with considerably distorted pseudooctahedral geometry. The two 1-phenylcyclohexanecarboxylate ligands coordinate the two iron atoms in an asymmetric manner with one Fe−O distance longer than the other (Table 2). The Fe···Fe distance is 3.738(4) Å.

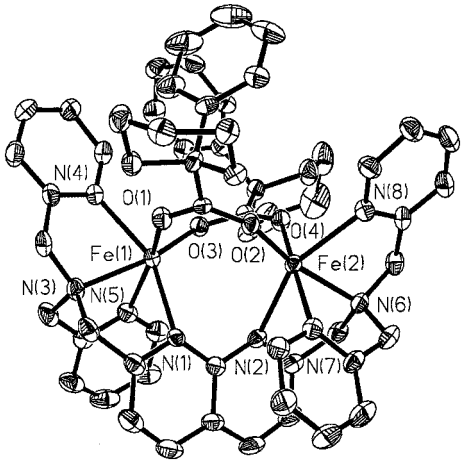

Figure 3. ORTEP diagram of [Fe_2(BPMAN)(μ-O_2CPhCy)$_2$](OTf)$_2$ (**1**) showing the 40% probability thermal ellipsoids for all non-hydrogen atoms.

Compound **2** was synthesized by a similar procedure, and green crystals were obtained from CH_2Cl_2/Et_2O at room temperature. A single-atom hydroxide bridge draws the two iron atoms together, the Fe···Fe distance being 3.221(6) Å. The carboxylate group and the 1,8-naphthyridine unit of BPMAN also link the iron atoms, the resulting Fe−O−Fe angle being 107.8(3)°. Each iron atom is six-coordinate with distorted pseudooctahedral geometry. The structure of **2** is shown in Figure 4, and selected bond lengths and angles are listed in Table 2. Compound **3**, a dimanganese(II) analogue of **1**, was also prepared and characterized. The two manganese atoms are 3.829(4) Å apart from each other, and details of the structure are included in Supporting Information.

Preparation and Structural Characterization of Paddle-Wheel Diiron(II) Complexes [Fe_2(BEAN)(μ-O_2CPhCy)$_3$](OTf) (4) and [Fe_2(BEAN)(μ-O_2CPh_3)$_3$](OTf) (5). The diiron(II) compound **4** was synthesized by allowing $Fe(OTf)_2 \cdot 2CH_3CN_3$, NaO_2CPhCy, and BEAN to react in a 2:3:1 ratio in tetrahydrofuran and crystallized as yellow blocks from pentane/Et_2O/CH_2Cl_2. X-ray crystallographic analysis revealed a paddle-wheel structure with two iron atoms bridged by three carboxylate groups and the 1,8-naphthyridine unit of ligand BEAN, as indicated in Figure 5. Each iron has a five-coordinate, square pyramidal stereochemistry and the Fe···Fe distance is 2.8486-(6) Å. The bridging 1-phenylcyclohexanecarboxylate ligands coordinate the two iron atoms with average Fe−O distances of 2.041(2) Å for Fe(1) and 2.030(2) Å for Fe(2) (Table 3). When NaO_2CCPh_3 was used as the carboxylate ligand, compound **5**

(21) *SMART v5.05*; Bruker AXS: Madison, WI, 1998.
(22) Feig, A. L.; Bautista, M. T.; Lippard, S. J. *Inorg. Chem.* **1996**, *25*, 6892−6898.
(23) Sheldrick, G. M. *SHELXTL97−2: Program for the Refinement of Crystal Structures*; University of Göttingen: Göttingen, Germany, 1997.
(24) Sheldrick, G. M. *SADABS: Area-Detector Absorption Correction*; University of Göttingen: Göttingen, Germany, 1996.
(25) Spek, A. L. *PLATON, A Multipurpose Crystallographic Tool*; Utrecht University: Utrecht, The Netherlands. 1998.
(26) Kent, T. A. *WMOSS: Mössbauer Spectral Analysis Software. 2.5*; Minneapolis, MN, 1998.

Table 1. Summary of X-ray Crystallographic Data

	1	**2**·CH_2Cl_2	**3**	**4**·CH_2Cl_2	**6**·CH_3CN
formula	$C_{62}H_{62}N_8O_{10}F_6S_2Fe_2$	$C_{50}H_{50}N_8O_9Cl_2F_6S_2Fe_2$	$C_{62}H_{62}N_8O_{10}F_6S_2Mn_2$	$C_{59}H_{75}N_4O_9Cl_2F_3SFe_2$	$C_{52}H_{53}N_9O_{10}F_6S_2Fe_2$
fw	1369.02	1267.70	1367.20	1255.89	1253.85
space group	$P2_1/c$	$P2_12_12_1$	$P\bar{1}$	$P2_1/n$	$P2_12_12$
a, Å	14.2124(3)	10.2490(3)	13.5590(4)	10.89270(10)	15.6105(5)
b, Å	22.3326(3)	21.7275(5)	14.6503(4)	38.5562(5)	32.7813(11)
c, Å	19.5692(4)	24.6524(7)	18.3921(6)	14.9577(2)	11.6641(4)
α, deg			82.0690(10)		
β, deg	95.4630(10)		70.0740(10)	110.0740(4)	
γ, deg			64.6370(10)		
V, Å^3	6183.0(2)	5489.7(3)	3103.54(16)	5900.32(12)	5968.9(3)
Z	4	4	2	4	4
T, °C	−85	−85	−85	−85	−85
ρ_{calcd}, g/cm^3	1.471	1.534	1.463	1.414	1.395
μ(Mo Kα), mm^{-1}	0.620	0.784	0.557	0.686	0.636
2θ range, deg	3−50	3−45	3−46	3−50	3−46
total no. of data	31849	23386	13760	43904	26553
no. of unique data	10866	7155	8572	10376	8307
observed data[a]	7035	5906	6151	8284	7129
no. of parameters	804	629	811	721	727
R[b]	0.0658	0.0769	0.0548	0.0445	0.0631
wR^2[c]	0.1660	0.2038	0.1415	0.1254	0.1558
max, min peaks, e/Å^3	0.828, −0.801	0.885, −0.948	0.777, −0.455	0.421, −0.652	0.963, −0.609

[a] Observation criterion: $I > 2\sigma(I)$. [b] $R = \sum||F_o| - |F_c||/\sum|F_o|$. [c] $wR^2 = \{\sum[w(F_o^2 - F_c^2)^2]/\sum[w(F_o^2)^2]\}^{1/2}$.

Table 2. Selected Bond Lengths (Å) and Angles (deg) for **1** and **2**·CH_2Cl_2[a]

	bond length		bond angle	
1	Fe(1)···Fe(2)	3.738(4)	O(1)−Fe(1)−O(3)	108.25(13)
	Fe(1)−O(1)	2.083(3)	O(1)−Fe(1)−N(1)	90.48(13)
	Fe(1)−O(3)	1.997(3)	O(1)−Fe(1)−N(5)	161.43(14)
	Fe(1)−N(1)	2.301(4)	O(3)−Fe(1)−N(3)	159.60(14)
	Fe(1)−N(3)	2.240(4)	N(1)−Fe(1)−N(3)	76.11(14)
	Fe(1)−N(4)	2.217(4)	N(1)−Fe(1)−N(4)	150.04(14)
	Fe(1)−N(5)	2.210(4)	O(2)−Fe(2)−O(4)	102.73(14)
	Fe(2)−O(2)	1.989(3)	O(2)−Fe(2)−N(2)	119.10(13)
	Fe(2)−O(4)	2.087(3)	O(2)−Fe(2)−N(6)	161.29(13)
	Fe(2)−N(2)	2.363(4)	O(4)−Fe(2)−N(7)	165.26(14)
	Fe(2)−N(6)	2.244(4)	N(2)−Fe(2)−N(6)	74.50(14)
	Fe(2)−N(7)	2.159(4)	N(2)−Fe(2)−N(8)	147.93(15)
	Fe(2)−N(8)	2.228(4)		
2·CH_2Cl_2	Fe(1)···Fe(2)	3.221(6)	Fe(1)−O(1)−Fe(2)	107.8(3)
	Fe(1)−O(1)	1.952(6)	O(1)−Fe(1)−O(2)	99.1(2)
	Fe(1)−O(2)	2.131(6)	O(1)−Fe(1)−N(1)	104.6(3)
	Fe(1)−N(1)	2.318(8)	O(1)−Fe(1)−N(3)	174.8(3)
	Fe(1)−N(3)	2.252(7)	O(2)−Fe(1)−N(4)	162.0(3)
	Fe(1)−N(4)	2.216(7)	N(1)−Fe(1)−N(3)	74.5(3)
	Fe(1)−N(5)	2.187(8)	N(1)−Fe(1)−N(5)	149.7(3)
	Fe(2)−O(1)	2.034(6)	O(1)−Fe(2)−O(3)	93.3(2)
	Fe(2)−O(3)	2.059(6)	O(1)−Fe(2)−N(2)	87.7(3)
	Fe(2)−N(2)	2.272(9)	O(1)−Fe(2)−N(8)	165.9(3)
	Fe(2)−N(6)	2.277(7)	O(3)−Fe(2)−N(6)	152.9(3)
	Fe(2)−N(7)	2.174(8)	N(2)−Fe(2)−N(6)	75.4(3)
	Fe(2)−N(8)	2.248(9)	N(2)−Fe(2)−N(7)	149.3(3)

[a] Numbers in parentheses are estimated standard deviations of the last significant figure. Atoms are labeled as indicated in Figures 3 and 4.

was obtained but only in low yield. There are two molecules in the asymmetric unit, one having severely disordered phenyl rings. Both molecules have the paddle-wheel diiron core and the structure of the ordered molecule is depicted in the Supporting Information.

Preparation and Structural Characterization of $[Fe_2(BBBAN)(\mu\text{-}OAc)_2(OTf)]$-(OTf) (6). The reaction of equal molar quantities of $Fe(OTf)_2 \cdot 2CH_3CN_3$, $Fe(OAc)_2$, and BBBAN in acetonitrile, followed by crystallization from Et_2O/CH_3CN, yielded crystals of **6**, the structure of which is shown in Figure 6. Selected bond lengths and angles are included in Table 3. Each iron is six-coordinate with pseudooctahedral geometry.

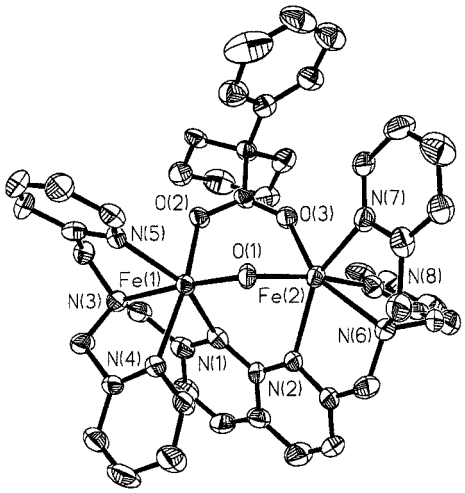

Figure 4. ORTEP diagram of $[Fe_2(BPMAN)(\mu\text{-}OH)(\mu\text{-}O_2CPhCy)](OTf)_2$ (**2**) showing the 40% probability thermal ellipsoids for all non-hydrogen atoms.

The two iron atoms are 3.504(4) Å apart and bridged by two acetates and the 1,8-naphthyridine unit of BBBAN. One acetate bridges two iron in a syn−syn bidentate fashion. The other acetate is monodentate bridging with coordination of the other oxygen atom O(4) to Fe(2). One triflate is terminally bound to Fe(1). The two acetate groups bridge two iron atoms such as those of residues Glu-144 and Glu-243 between the two iron(II) atoms in reduced MMOH (Figure 1).

Electrochemistry of 1. The cyclic voltammogram (CV) of **1**, recorded in CH_2Cl_2, exhibits two reversible redox waves with $E_{1/2}$ values of +296 mV (ΔE_p = 80 mV) and +781 mV (ΔE_p = 74 mV) vs Cp_2Fe^+/Cp_2Fe (Figure 7). This result implies that the diiron(II,III) and diiron(III) states may be accessed chemically and electrochemically from **1**. Self-assembled diiron centers typically dissociate when undergoing redox reactions, although one-electron reversible redox waves have been previously reported for carboxylate-bridged diiron centers with or without single-atom bridge(s).[27−30] The observation of two reversible redox waves is unprecedented to our knowledge for a carboxylate-supported diiron center without any single-atom bridge, however.

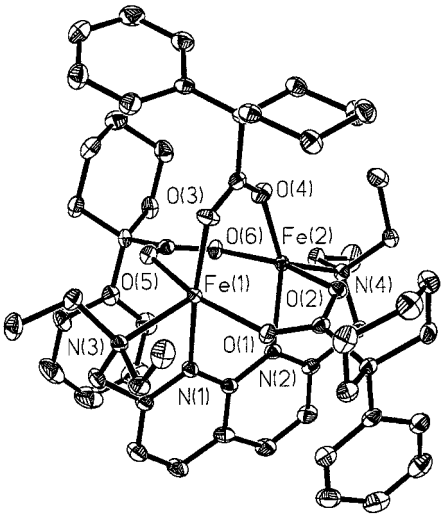

Figure 5. ORTEP diagram of $[Fe_2(BEAN)(\mu\text{-}O_2CPhCy)_3](OTf)$ (**4**) showing the 40% probability thermal ellipsoids for all non-hydrogen atoms.

Table 3. Selected Bond Lengths (Å) and Angles (deg) for **4**·CH_2Cl_2 and **6**·CH_3CN[a]

	bond length		bond angle	
4·CH_2Cl_2	Fe(1)···Fe(2)	2.8486(6)	O(1)−Fe(1)−O(3)	91.73(8)
	Fe(1)−O(1)	2.0370(19)	O(1)−Fe(1)−O(5)	157.57(8)
	Fe(1)−O(3)	2.056(2)	O(3)−Fe(1)−O(5)	91.81(8)
	Fe(1)−O(5)	2.0312(19)	O(1)−Fe(1)−N(3)	105.13(9)
	Fe(1)−N(1)	2.179(2)	O(3)−Fe(1)−N(1)	171.79(9)
	Fe(1)−N(3)	2.167(2)	O(3)−Fe(1)−N(3)	109.38(9)
	Fe(2)−O(2)	2.0496(19)	O(2)−Fe(2)−O(4)	90.30(8)
	Fe(2)−O(4)	2.034(2)	O(2)−Fe(2)−O(6)	163.68(8)
	Fe(2)−O(6)	2.0051(19)	O(4)−Fe(2)−O(6)	87.81(8)
	Fe(2)−N(2)	2.210(2)	O(2)−Fe(2)−N(2)	86.92(8)
	Fe(2)−N(4)	2.153(2)	O(4)−Fe(2)−N(2)	152.78(9)
			O(4)−Fe(2)−N(4)	129.15(9)
6·CH_3CN	Fe(1)···Fe(2)	3.504(4)	Fe(1)−O(3)−Fe(2)	106.17(18)
	Fe(1)−O(1)	2.050(5)	O(1)−Fe(1)−O(3)	90.30(17)
	Fe(1)−O(3)	2.112(4)	O(1)−Fe(1)−O(5)	177.4(2)
	Fe(1)−O(5)	2.130(5)	O(1)−Fe(1)−N(1)	102.15(19)
	Fe(1)−N(1)	2.315(5)	O(3)−Fe(1)−N(3)	167.78(19)
	Fe(1)−N(3)	2.245(6)	N(1)−Fe(1)−N(3)	74.65(19)
	Fe(1)−N(4)	2.165(5)	N(1)−Fe(1)−N(4)	162.4(2)
	Fe(2)−O(2)	1.981(5)	O(2)−Fe(2)−O(3)	106.38(17)
	Fe(2)−O(3)	2.268(4)	O(2)−Fe(2)−O(4)	165.27(18)
	Fe(2)−O(4)	2.160(4)	O(3)−Fe(2)−O(4)	58.90(16)
	Fe(2)−N(2)	2.304(5)	O(2)−Fe(2)−N(2)	94.67(19)
	Fe(2)−N(6)	2.189(5)	O(3)−Fe(2)−N(6)	146.00(18)
	Fe(2)−N(7)	2.155(5)	N(2)−Fe(2)−N(7)	169.11(19)

[a] Numbers in parentheses are estimated standard deviations of the last significant figure. Atoms are labeled as indicated in Figures 5 and 6.

The presence of two anionic carboxylate groups and the neutral 1,8-naphthyridine moiety in bridging positions between the diiron centers in **1** is consistent with the high oxidation potentials exhibited. The self-assembled tetracarboxylate diiron(II) compound $[Fe_2(\mu\text{-}O_2CAr^{Tol})_4(4\text{-}^tBuC_5H_4N)_2]$, recently reported from our laboratory, undergoes a reversible one-electron

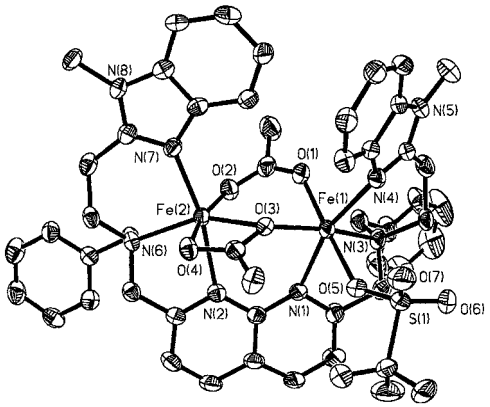

Figure 6. ORTEP diagram of $[Fe_2(BBBAN)(\mu\text{-}OAc)_2(OTf)](OTf)$ (**6**) showing the 40% probability thermal ellipsoids for all non-hydrogen atoms.

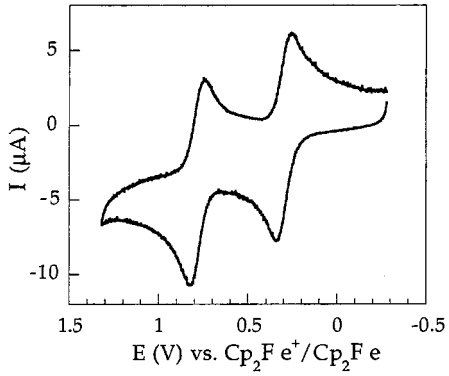

Figure 7. Cyclic voltammogram of 2 mM $[Fe_2(BPMAN)(\mu\text{-}O_2CPhCy)_2](OTf)_2$ (**1**) in CH_2Cl_2 with 0.5 M $(Bu_4N)(PF_6)$ as supporting electrolyte and a scan rate of 100 mV/s.

oxidation with an $E_{1/2}$ value of −216 mV vs Cp_2Fe^+/Cp_2Fe in CH_2Cl_2.[29] A mixed-valence diiron(II,III) complex with two five-coordinate iron atoms was obtained from this oxidation. A short metal−metal distance of 2.6982(13) Å suggested direct interaction between two iron centers in the mixed-valence form. With two additional anionic carboxylate groups, the oxidation potential of the diiron(II) center in this system is 512 mV lower than that of **1**, suggesting that the addition of each anionic carboxylate group causes an approximately −250 mV change of the redox potential of a diiron center. Further oxidation of the tetracarboxylate-bridged diiron(II,III) species was not observed by cyclic voltammetry, however. The presence of the second redox couple in the CV of **1** therefore suggests that a diiron(III) species with carboxylate-only anionic bridges could be feasible if the diiron unit were stabilized by the use of a multidentate ligand system.

By using alkoxide-bridged heptadentate dinucleating ligands BPMP and BIMP, two reversible redox waves were previously observed for diiron(II) complexes having two additional carboxylate bridges (Table 4).[31−34] The $E_{1/2}$ values for the $Fe^{III}Fe^{II}/Fe^{II}Fe^{II}$ and $Fe^{III}Fe^{III}/Fe^{III}Fe^{II}$ couples of these complexes measured in acetonitrile are several hundred millivolts lower than those of **1** when converted to approximately the same scale (Table 4). The alkoxide bridge, not yet found in a biological

(27) Hartman, J. R.; Rardine, R. L.; Chaudhuri, P.; Pohl, K.; Wieghardt, K.; Nuber, B.; Weiss, J.; Papaefthymiou, G. C.; Frankel, R. B.; Lippard, S. J. *J. Am. Chem. Soc.* **1987**, *109*, 7387−7396.
(28) Holz, R. C.; Elgren, T. E.; Pearce, L. L.; Zhang, J. H.; O'Connor, C. J.; Que, L., Jr. *Inorg. Chem.* **1993**, *32*, 5844−5850.
(29) Lee, D.; Krebs, C.; Huynh, B. H.; Hendrich, M. P.; Lippard, S. J. *J. Am. Chem. Soc.* **2000**, *122*, 5000−5001.
(30) Que, L., Jr.; True, A. E. In *Progress in Inorganic Chemistry*; Lippard, S. J., Eds.; John Wiley & Sons: New York, 1990; Vol. 38, pp 97−200.
(31) Suzuki, M.; Uehara, A.; Oshio, H.; Endo, K.; Yanaga, M.; Kida, S.; Saito, K. *Bull. Chem. Soc. Jpn.* **1987**, *60*, 3547−3555.
(32) Borovik, A. S.; Papaefthymiou, V.; Taylor, L. F.; Anderson, O. P.; Que, L., Jr. *J. Am. Chem. Soc.* **1989**, *111*, 6183−6195.
(33) Mashuta, M. S.; Webbs, R. J.; Oberhausen, K. J.; Richardson, J. F.; Buchanan, R. M.; Hendrickson, D. N. *J. Am. Chem. Soc.* **1989**, *111*, 2745−2746.

Table 4. Redox Potential of Diiron Centers in Complexes **1** and **2** and Selected Previous Models

complex	$Fe^{III}Fe^{III}/Fe^{III}Fe^{II}$ (mV vs SCE)[a]	$Fe^{III}Fe^{II}/Fe^{II}Fe^{II}$ (mV vs SCE)[a]	ref
$[Fe_2O(OAc)_2(Me_3TACN)_2](PF_6)$	−370[b]	−1500[c]	27
$[Fe_2O(OAc)_2(TPA)_2](ClO_4)_2$	−90		28
$[Fe_2(BPMP)(OAc)_2](BF_4)_2$	+680	−30	31
$[Fe_2(BPMP)(OAc)_2(OH)](BF_4)_2$	+670	−80	31
$[Fe_2(BPMP)(OPr)_2](BPh_4)_2$	+692	−10	32
$[Fe_2(BIMP)(OAc)_2](ClO_4)_2$	+435	−245	33
$[Fe_2(\mu\text{-}O_2CAr^{Tol})_4(4\text{-}^tBuC_5H_4N)_2]$		+244	29
1	+1241	+758	this work
2		+438	this work

[a] Cp_2Fe^+/Cp_2Fe = +460 mV vs SCE in CH_2Cl_2. [b] Quasireversible. [c] Irreversible.

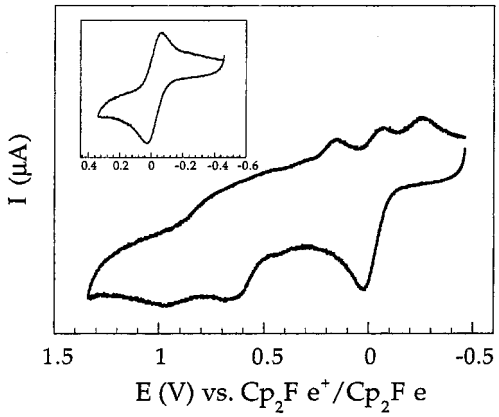

Figure 8. Cyclic voltammogram of 2 mM $[Fe_2(BPMAN)(\mu\text{-}OH)(\mu\text{-}O_2CPhCy)](OTf)_2$ (**2**) in CH_2Cl_2 with 0.5 M $(Bu_4N)(PF_6)$ as supporting electrolyte and a scan rate of 100 mV/s. The insert shows the reversible wave observed when the experiment was conducted at potentials below +400 mV vs Cp_2Fe^+/Cp_2Fe.

system, significantly decreases the redox potential of the diiron core.

A similar bis(μ-carboxylato)diiron(II) complex, $[Fe_2(\mu\text{-}O_2CCH_3)_2(TPA)_2](BPh_4)_2$, was synthesized to model the reduced forms of diiron-containing enzymes.[9,35] This compound, prepared by self-assembly from an iron(II) precursor and TPA, is very O_2 reactive. By contrast, a CH_2Cl_2 solution of **1** reacts with O_2 very slowly (several days) at room temperature. Thus the dinucleating ligand used here, while stabilizing the dinuclear iron core under different redox conditions, limits its O_2 reactivity, possibly due to its more rigid geometry, which prevents it from forming monomers in solution. It was suggested that $[Fe_2(\mu\text{-}O_2CCH_3)_2(TPA)_2](BPh_4)_2$ does dissociate in solution, which may contribute to its greater reactivity.

Electrochemistry of 2 and 3. A carboxylato- and hydroxo-bridged diiron(II) complex **2** was prepared in which a hydroxide group has replaced one of the two carboxylate bridges in **1**. The cyclic voltammogram of **2** recorded in CH_2Cl_2 exhibited a reversible redox wave at −22 mV (ΔE_p = 84 mV) when the CV experiment was conducted at potentials below +400 mV vs Cp_2Fe^+/Cp_2Fe (Figure 8, inset). When the scan range was extended to higher potentials, a second reversible wave was not observed. Instead, the reduction wave of the original reversible couple at −22 mV split into three components, as shown in Figure 8. An irreversible redox process occurred when CV experiments were conducted in the presence of 5 equiv of Et_3N at potentials below +400 mV. These results suggest that the reversible wave at −22 mV may correspond to the Fe(III)−OH−Fe(II)/Fe(II)−OH−Fe(II) couple. The electrochemistry becomes irreversible when both iron atoms are oxidized at higher potentials, possibly due to core disassembly. In the presence of excess base, the hydroxide bridge may be deprotonated upon oxidation of one of the iron atoms, rendering the previously reversible process irreversible. The oxidation potential for the $Fe^{III}Fe^{II}/Fe^{II}Fe^{II}$ couple of **2** is approximately 318 mV lower than that of **1**. The presence of a more donating hydroxide bridge in **2** makes the diiron center easier to oxidize.

The CV of **3**, a dimanganese(II) analogue of **1**, was also recorded in dichloromethane. The dimetallic center was only oxidized at around 960 mV, and an irreversible process was observed (Supporting Information).

Compounds **4** and **5** resemble the tetracarboxylate-bridged paddle wheel complex $[Fe_2(\mu\text{-}O_2CAr^{Tol})_4(4\text{-}^tBuC_5H_4N)_2]$ reported recently,[29] with one carboxylate bridge being replaced by the 1,8-naphthyridine unit of BEAN. The CV of **4** showed only irreversible electrochemistry with oxidation only at potentials above +400 mV vs Cp_2Fe^+/Cp_2Fe (Supporting Information). This result may be contrasted with the reversible redox behavior of $[Fe_2(\mu\text{-}O_2CAr^{Tol})_4(4\text{-}^tBuC_5H_4N)_2]$ in CH_2Cl_2 at an $E_{1/2}$ value of −216 mV vs Cp_2Fe^+/Cp_2Fe. The additional carboxylate group may play an important role in stabilizing the five-coordinate mixed-valence diiron(II,III) oxidation product in the tetracarboxylate-bridged system. Complex **4** is also unreactive toward O_2 in CH_2Cl_2 at room temperature, although potential coordination sites are available. The rigid ligand scaffold may limit access of a potential O_2-derived ligand to the available coordination site. The CV result also implies that compound **4** cannot be oxidized by O_2 by an outer sphere electron transfer. The diiron(II) complex $[Fe_2(\mu\text{-}O_2CAr^{Tol})_4(4\text{-}^tBuC_5H_4N)_2]$, with a lower oxidation potential, reacts with O_2 to give a mixture of diiron(II,III) and diiron(III,IV) species at −78 °C.[14]

The CV of **6** was also recorded in CH_2Cl_2. An irreversible process was observed at potentials above +400 mV vs Cp_2Fe^+/Cp_2Fe (Supporting Information). The hexadentate ligand BBAAN appears not to stabilize the diiron core as effectively as the octadentate ligand BPMAN when the oxidation states of the metals change. A solution of compound **6** in acetonitrile or CH_2Cl_2 is O_2 sensitive, presumably because dissociation of triflate provides easy access of O_2 to the diiron unit.

Mössbauer Spectroscopic Studies. Mössbauer spectra of **1**, **2**, **4**, **6**, and **7** in the solid state were recorded at 4.2 K. Parameters are summarized in Table 5. A fit of the data for **1** gives values for the diiron(II) state of δ = 1.18(2) mm/s and ΔE_Q = 3.01(2) mm/s. The Mössbauer parameters of **2**, with average values of δ_{av} = 1.15(2) mm/s and ΔE_{Qav} = 2.80(2) mm/s, compare very well with those of deoxyHr (δ = 1.14 mm/s and ΔE_Q = 2.76(2) mm/s).[30] The spectra of **1** and **2** are illustrated in Figure 9.

(34) BPMP = 2,6-bis[(bis(2-pyridylmethyl)amino)methyl]-4-methylphenol and BIMP = 2,6-bis[(bis((1-methylimidazolyl)methyl)amino)methyl]-4-methylphenol.
(35) TPA = tri(2-pyridylmethyl)amine.

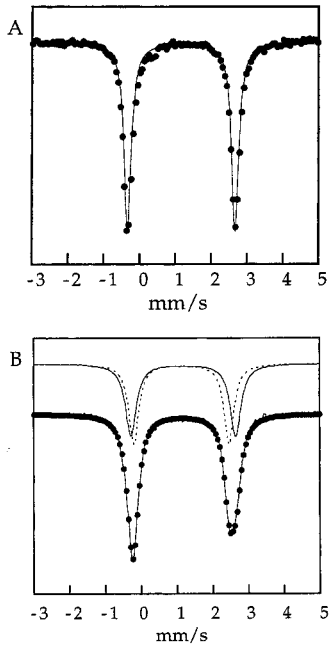

Figure 9. Mössbauer spectra at 4.2 K of (A) $[Fe_2(BPMAN)(\mu\text{-}O_2CPhCy)_2](OTf)_2$ (**1**) and (B) $[Fe_2(BPMAN)(\mu\text{-}OH)(\mu\text{-}O_2CPhCy)](OTf)_2$ (**2**). Lower curves: experimental data (·) and calculated fit (−). Upper curves: subsets for the calculated spectrum of **2**.

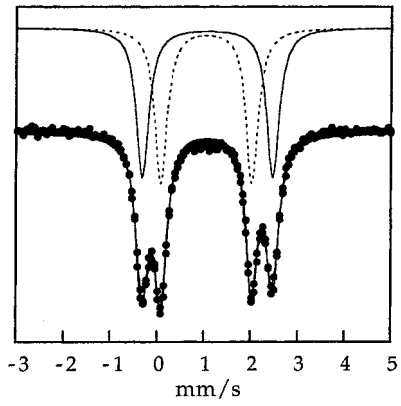

Figure 10. Mössbauer spectra at 4.2 K of $[Fe_2(BEAN)(\mu\text{-}O_2CPhCy)_3](OTf)$ (**4**). Lower curves: experimental data (·), calculated fit (−). Upper curves: two subsets for the calculated spectrum.

Table 5. Summary of Mössbauer Parameters for **1**, **2**, **4**, and **6** Recorded at 4.2 K (mm/s) in the Solid State

complex	d	ΔE_Q	G
1 (powder)	1.18(2)	3.01(2)	0.24(2)
2 (powder)	1.13(2)	2.66(2)	0.33(2)
	1.18(2)	2.93(2)	0.37(2)
4 (powder)	1.05(2)	1.95(2)	0.31(2)
	1.08(2)	2.79(2)	0.32(2)
6 (powder)	1.20(2)	3.28(2)	0.35(2)
	1.24(2)	3.03(2)	0.35(2)

The spectrum of **4** shows two distinct iron sites, one having $\delta = 1.05(2)$ mm/s and $\Delta E_Q = 1.95(2)$ mm/s and the other having $\delta = 1.08(2)$ mm/s and $\Delta E_Q = 2.79(2)$ mm/s (Figure 10). The large difference of the quadrupole splitting values between two iron sites, although not fully understood, may arise from the more asymmetric environment of Fe(2) (Table 3). The Mössbauer parameters of **6**, listed in Table 5, are closer to those exhibited by the active site of H_{red} of MMO ($\delta = 1.30$ mm/s and $\Delta E_Q = 2.87-3.14$ mm/s), probably because they have similar carboxylate bridging modes.[36,37]

Summary and Conclusions

Several carboxylato- and 1,8-naphthyridine-bridged diiron(II) complexes were prepared and characterized by using 1,8-naphthyridine-based dinucleating ligands. The cyclic voltammograms and Mössbauer spectra of these compounds were recorded. The bis(μ-carboxylato)(μ-1,8-naphthyridine)diiron(II) complex $[Fe_2(BPMAN)(\mu\text{-}O_2CPhCy)_2]\text{-}(OTf)_2$ (**1**) exhibited two one-electron reversible redox waves, which are assigned to the $Fe^{III}Fe^{II}/Fe^{II}Fe^{II}$ and $Fe^{III}Fe^{III}/Fe^{III}Fe^{II}$ couples, respectively. Such behavior has only been previously encountered for diiron complexes derived from alkoxide-bridged multidentate ligands and is unprecedented for carboxylate-linked complexes having no single-atom bridge. The results suggest that diiron(II) sites bridged only by carboxylate groups in biology can act to supply one to two electrons without a significant change of geometry. The oxidation potentials of **1** are quite high. Comparison with results from a previously reported tetracarboxylate-bridged diiron(II) compound indicates that addition of two anionic carboxylate groups shifts the first oxidation potential of the diiron(II) unit by approximately −512 mV. With additional imidazole donor ligands and in the protein environment, the diiron(II) cores at the active sites of the enzymes have much lower oxidation potentials that fall into the physiological range, by comparison to these model complexes.

The cyclic voltammograms of the carboxylato- and hydroxo-bridged diiron complex $[Fe_2(BPMAN)(\mu\text{-}OH)(\mu\text{-}O_2CPhCy)]\text{-}(OTf)_2$ (**2**) exhibited one reversible redox wave at −22 mV, only when the CV experiment was conducted at potentials below +400 mV vs Cp_2Fe^+/Cp_2Fe in CH_2Cl_2. The much lower oxidation potential of **2** compared to **1** is consistent with replacement of one carboxylate bridge with a more donating hydroxide ion. The dimanganese(II) complex $[Mn_2(BPMAN)(\mu\text{-}O_2CPhCy)_2](OTf)_2$ (**3**), an analogue of **1**, could not be oxidized at potentials below +900 mV. At higher potentials, an irreversible process occurred. Thus the two reversible redox waves below +900 mV exhibited by **1** can be attributed to the diiron core; ligand oxidation most likely can be excluded.

Diiron(II) complexes $[Fe_2(BEAN)(\mu\text{-}O_2CPhCy)_3](OTf)$ (**4**), $[Fe_2(BEAN)(\mu\text{-}O_2CCPh_3)_3](OTf)$ (**5**), and $[Fe_2(BBBAN)(\mu\text{-}OAc)_2(OTf)](OTf)$ (**6**) were also synthesized and characterized. No oxidation occurs in CH_2Cl_2 solutions of complexes **4** and **6** at potential below +400 mV vs Cp_2Fe^+/Cp_2Fe, as judged from CV experiments. Complex **4** is O_2 inert, whereas **6** is sensitive to O_2 in solution. The rigid geometry that restrains access of O_2 to the diiron core may account for the lack of O_2 reactivity of **4**, whereas an open coordination site in **6** may provide an O_2 binding site.

Acknowledgment. This work was supported by grants from the National Science Foundation and National Institute of General Medical Sciences. We thank Mr. Dongwhan Lee and Ms. Jane Kuzelka for help in acquiring and fitting the Mössbauer spectra.

Supporting Information Available: Figure S1, showing the ORTEP diagram of **3**; Figure S2, the connectivity of **5**; Figures S3−S7, the cyclic voltammograms of **1**, **2** in the presence of excess Et_3N, **3**, **4**, and **6**; and Figure S9, the Mössbauer spectrum of **6**; and X-ray crystallographic files, in CIF format, for complexes **1**−**4** and **6**. This material is available free of charge via the Internet at http://pubs.acs.org.

IC000975K

(36) Liu, K. E.; Valentine, A. M.; Wang, D.; Huynh, B. H.; Edmondson, D. E.; Salifoglou, A.; Lippard, S. J. *J. Am. Chem. Soc.* **1995,** *117*, 10174−10185.
(37) Fox, B. G.; Surerus, K. K.; Münck, E.; Lipscomb, J. D. *J. Biol. Chem.* **1988**, *263*, 10553−10556.